DOR: 20.1001.1.27170314.2023.12.3.1.8

Research Paper

Improving the Efficiency and Durability of Blast Furnace Air Tuyere Through Different Ceramic Coating Materials

Hasan Bagheri Hasan Abadi[1], Mohsen Hamedi[2*]
[1]PhD. Candidate, Kish International Campus, University of Tehran, Kish, Iran
[2]Professor, School of Mechanical Engineering, University of Tehran, 1450 North Kargar Avenue, 14399-57131, Iran
*Email of Corresponding Author: mhamedi@ut.ac.ir
Received: July 13, 2023; Accepted: August 29, 2023

Abstract
Blast air tuyeres are one of the critical components of a blast furnace that are exposed to severe conditions caused by thermal shocks, mechanical erosion, hot chemical corrosion, wettability caused by penetration of molten cast iron, and cracks caused by the thermal cycle. These factors decrease the lifetime of air tuyeres, causing unpredictable failure and costly production stoppages. The present study investigates the protection performance of three types of atmospheric plasma-sprayed ceramic coatings on air tuyeres against the harsh operating environment. As the substrate of air tuyeres, 99.95% pure copper is coated with Yttria Stabilized Zirconia YSZ8%, alumina-zirconia (AZ) and alumina-magnesia (AM). The performance of these three coatings was evaluated using mechanical wear and erosion tests, chemical hot corrosion tests, micro-hardness adhesion strength tests, and porosity measurements. Based on the results, AZ and AM coatings generally performed better than YSZ8% coating in all above-mentioned tests excluding the adhesion strength test. In the adhesion strength test, the AZ coating performance was found to be close to that of YSZ8% coating. Meanwhile, in the mechanical erosion and wear tests, the AM coating outperformed and underperformed the AZ coating, respectively. The porosity of AZ coating was also close to that of AM coating. Hence, it is expected that the blast air tuyere with AZ and AM coatings can offer better performance in blast furnace due to their superior metallurgical and mechanical properties. However, in practice, the AZ coating outperformed the AM coating in BF due to a three-fold increase in the lifecycle.

Keywords
Blast Air Tuyere, Mechanical and Chemical Hot Corrosion, Degradation Test, Thermal Degradation Test, Thermal Spray Coating

1. Introduction

Considering the advantages and disadvantages, indirect reduction (blast furnace) and direct reduction are the two practical methods for commercial steel production. Nearly 70% of the steel production worldwide is accredited to the indirect reduction method, thus, its high contribution to the steel industry. In this method, iron ore is fed into the BF along with coke and other materials, and oxygen-enriched air is blown into the furnace at about 1250 °C through the air tuyeres. In this process, the

coke ignition produces the cast iron, followed by the iron ore melting and recovery. The air tuyere is made of a 99.95% pure copper cathode manufactured by casting.

Blast air tuyere is one of the most vital components of a blast furnace, where any failure will lead to BF shut-down [1]. These components are exposed to thermal shocks, mechanical abrasion, and chemical hot corrosion, especially in the nose area. Mechanical abrasion is caused by the raw material impact, coke eddy motion, metal and slag particles, and hot particles [2-4]. According to [5], tuyere damage occurs mainly because of erosion and hot metal burnout. Hot chemical corrosion is caused by acidic chemical corrosive gases like the sulfur and chlorine produced by the coal-burning or the oxidation of metal sulfides during raw materials feeding and non-acidic metal vapors like cadmium, lead, zinc, etc. [4-6]. Copper sulfide is yield from a sulfur reaction.

One of the most important causes of damage to air tuyeres is wettability due to the penetration of molten cast iron and slag. Cracking, which commonly occurs inside the body of the tuyere after a period of operation of the tuyere subject to a hot and cold thermal cycle, contributes to tuyere damage. Increased cracking inside the body of tuyere will lead to water leakage [4]. One or a combination of the preceding factors might cause tuyere failure leading to the BF shut-down.

The blast is close to the boundary between the furnace's belly and bottom. Based on the air tuyere design, about one-third of the tuyere’s length (about 400 to 600 mm) from its tip projects into the furnace. The highest blast air temperature reaches 1250°C, while the temperature of the flame in front of tuyere reaches up to 2450°C [7]. Under such circumstances, each tuyere must continue the hot air transfer or blow next to maintain its original structure. The circulating water inside the tuyere cooling chambers cools down the tuyere that is in direct contact with the flame's heat and hot metal. Like any other system component, the air tuyeres are usually damaged, and the furnace must be shut down for replacement. The replacement process disrupts production due to significant direct and indirect economic losses. Any shut-downs account for up to 2-2.5% of BF operating time [6], next to increasing coke consumption [8,9].

About 70 years ago, Hirakawa noted that the tuyere damage due to its contact with hot metal is caused by excessive heating. Applying aluminum due to its good thermal conductivity, proper surface smoothness, workability, and lightweight compared to copper was suggested as a solution; nevertheless, since 1950, most tuyeres operating have been damaged. Following 1950, there has been a large-scale operation of BFs, resulting in high operation, high blast air temperatures, fuel oil, and oxygen injection. Due to its high productivity, pulverized coal injection (PCI) began in 1980. The high temperature on the BF air tuyere forehead and increased volume of hot metal and slag droplets contribute to a considerable increase in the thermal load on the tuyeres and, thus, frequent damage to the tuyeres [3,4,6,10]. A higher coal injection rate might increase the risk of damage to the tuyere [2]. Due to the increased temperature of the tuyere, more than 50% of the tuyere damage is attributed to temperature effect, high radiation absorption, low thermal conductivity, low cooling system, and operating parameters [11]. To allow the tuyere replacement and assure sustained operation, it is necessary to stop the oxygen-enriched air and fuel and remove the tuyere from its installation place that causes the production loss [7].

In recent years, the development of ceramic composite coatings on copper substrates has gained significant attention due to their potential for thermal insulation, corrosion protection, and enhanced material performance. This review explores key studies in this field, highlighting advancements,

challenges, and promising directions. A comprehensive investigation into the influence of granulometric composition in ceramic coatings on copper has underscored the critical role of particle size and distribution in achieving optimal coating properties [12]. Additionally, the exploration of sodium silicate binders revealed their impact on the overall performance of these coatings, shedding light on the importance of binder selection in achieving desired outcomes [13]. There also exists a thorough review that dissected the complex process of bonding formation during thermal spraying of ceramic coatings [14]. This review not only elucidated the mechanisms behind successful adhesion but also pointed to potential strategies for improving the bonding strength between ceramic coatings and copper substrates. A significant advancement was the study of plasma spraying techniques for creating alumina-yttria composite ceramic coatings on copper substrates was. Focusing on the electrical insulation applications, the mentioned study highlighted the multifaceted utility of these coatings beyond mere thermal protection [15]. Intriguingly, the realm of plasma-sprayed alumina ceramic coatings has also been appraised by exploring metastable phase formation, microstructure evolution, and dielectric properties [16] This appraisal contributes vital insights into the fundamental characteristics of these coatings, thereby paving the way for more tailored and optimized applications. A broader perspective was taken by investigating black oxide coatings across various metal substrates, including copper [17]. While not exclusively focused on ceramics, the findings have implications for understanding coating adhesion, durability, and protective properties on copper surfaces. A deeper understanding of plasma-sprayed copper-coated alumina substrates was also found [18]. Providing valuable knowledge for designing coatings that withstand real-world operating conditions, it delved into the intricate interplay between surface resistivity and bonding strength. Despite the wealth of knowledge derived from these studies, it is crucial to acknowledge that the operational context of air tuyeres, which is the central concern of this article, presents unique challenges that necessitate specific research.A thermal insulation ceramic coating is considered as an effective solution to prevent damage to the outer surface of the tuyere body [2,11,19].

Researchers in [20] applied a coating onto the inner and outer surface of the tuyere through the colorizing method. Consisting of a mixture of Al_2O_3 and Al powder, this coating reduced hot cast iron penetration in the tuyere, thus lowering the tuyere failure. Researchers in [21] coated the tuyere with a three-layer ceramic thermal insulation coating consisting of 1) the prime layer, a bonded layer made of Ni-based superalloy (NiCrAlY) or Co-based superalloy (CoCrAlY) spayed by applying plasma deposition technique, 2) a ceramic half primer made of bonded oxide-stabilized zirconia like y_2O_3, CaO, and MgO coated on the bonding layer by adopting the sputtering technique and 3) a half layer containing stabilized zirconia.

Researchers in [22] applied a three-layer alumina ceramic coating by applying a nickel-based bonded metal layer on a copper substrate [23]. Other researchers [24] applied a three-layer ceramic coating, where the first layer consists of a layer of nickel-based self-flux material, sprayed by plasma or oxy-acetylene flame spraying methods; the second and third layers consist of a mixture of alloys and ceramic materials. As to the metallurgical properties of the coating, the adhesion strength of ceramic coatings is of high significance.

The limited literature available underscores the need for more focused investigations within this specialized domain. In conclusion, the reviewed literature showcases the evolution of ceramic composite coatings on copper substrates, offering insights into materials, fabrication techniques, and

performance assessment. While existing studies provide a solid foundation, further research is warranted to bridge the gap between laboratory findings and practical application in air tuyere systems. One of the proposed methods of reducing the air tuyere damage is to apply a ceramic coating on the outer wall circumfrence of the tuyere. The coating adhesion strength prevents the rapid detachment and destruction and increases the coating layer life, consequently preventing the tuyere destruction and increasing its service life.

The AZ and AM powders with the compositions are shown in Table 1 are applied on 99.95% pure copper substrate as coating, which is covered by the well-known YSZ8% powder for the first time, to become subject to chemical hot corrosion, mechanical corrosion, and mechanical erosion and abrasion tests. The porosity and adhesion strength of these two coatings are measured. Alumina has high corrosion resistance (in both acidic and alkaline environments), high melting point, proper shock resistance, and high abrasion strength properties. The AM powder has high shock resistance, corrosion strength, and melting temperature (2135°C) [24].

Likewise, adding zirconia to the coating mixture has improved its resistance to crack propagation [22], which is cheaper than YSZ8%.

2. Materials and methods

2.1 Coating and substrate materials

The materials of the three ceramic thermal insulation coatings, the YSZ8%, and two AZ and AM ceramic powders with their chemical analysis are presented in Table 1. The NiCrAlY alloy is consumed as the bond layer powder.The YSZ8% powder is purchased from 2008-PAC-USA, AZ refractory powder from Treibacher-Aeser,Germany, AM powder from IREFCO, Iran, and NiCrAlY powder Amdry962 from Metco-Sulzer Inc.,USA. Both AZ and AM powders are consumed in their agglomerated form. Copper specimens with a purity of 99.95% and 6×34×34mm in dimensions are consumed to prepare the three ceramics and run the tests.

Table 1. Chemical analysis of ceramic AZ and AM powders (%)

Powder	Al_2O_3	MgO	SiO_2	ZrO_2	Na_2O	Fe_2O_3	CaO	TiO_2
Components								
AZ(%)	73	--	19	5.5	1	0.7	0.5	0.3
AM(%)	74-76	22-24	0.3	--	--	0.3	0.5	--

- *Coating deposition*

All these ceramic powder coatings and NiCrAlY bonding layer powder are sprayed by applying the plasma spray technique. A similar NiCrAlY bonding layer 100 ± 20 microns in thickness is coated on a separate copper substrate for three coatings. Next, one 200±50 micron layer is applied to the bonding layer from each ceramic powder. The parameters applied in atmospheric plasma spraying (APS) are presented in Table 2.

Table 2. Parameters used in plasma-sprayed coatings

Spray Parameters	Bonding Coating	YSZ Topcoat	AZ Topcoat	AM Topcoat
Arc Current (A)	600	600	450	600
Plasma Primary Gas Flowrate (Ar) (1/min)	65	35	35	35
Plasma Secondary Gas Flowrate (H_2) (1/min)	12	12	12	12
Flowrate of Powder Carrying Gas (Ar) (1/min)	2.3	3.5	3	3.5
Spray Distance (mm)	120	80	100	80
Pulverized Injection Rate (g/mm)	40	35	30	35

- *Coating specifications*

Surface and cross-sectional images are prepared from the coated specimen through electron microscopy MIRA3, TESCAN, and Czech, together with elemental surface analysis through electronic data systems (EDS). The Vickers micro-hardness values are measured from the surface of the coatings through the KB250 tester, Germany, with a 5 kg force. The mean porosity volumes are weighted at ten points through the image processing method from the surface and cross-sectional area of the coatings; to accomplish this, the electron microscope surface images, 200-micron scale, and cross-sectional images, 100-micron scale is put into the Image Analyzer software (Video TesT-Metal 1.2). Microhardness and porosity volumes are measured at ten points to determine the mean value. The analysis of the coating material is run by applying X-ray diffraction analysis (XRD) Asenware AW/XDM 300, China.

2.2 Assessing coating performance vs. mechanical erosion

The solid particle erosion tests are run on all coatings according to G76-024 subject to argon gas pressure at a 70 m/s velocity [25] where the silica sand particles are blasted on the surface of the coatings at two 30 and 90 angles. The weight loss is measured by four decimal place accuracy precise weighing, which indicates the mechanical erosion measure. The initial test is run on three specimens at each coating.

2.3 Assessing the coating performance vs. mechanical Wear

The wear tests are run on all coatings subject to ASTM G99, where the disc-shaped specimen is firmly fixed on the device subject to a 6 kg force on its surface. The disc begins rotating at a 45 turns/min velocity. The weight loss is measured by four decimal place accuracy in precise weighing. This value indicates the mechanical erosion measure.

2.4 Assessing performance vs. hot chemical corrosion

50wt% $FeCl_3$ together with 50wt% $FeSO_4$ is spread evenly on the coating surface of the specimens with a 25 mg/cm^2 distribution. The specimens are placed in an oven at 850 °C for 40 hours. After being cooled to room temperature, the chemical corrosion is tested through X-ray diffraction (XRD) based on the residual compounds on the coatings.

2.5 Electrochemical tests

- Polarization test

In this study, the potentiodynamic polarization spectroscopy test was performed using a potentiostat device of IVIUM Electrochemical System model.The method was based on the classical cell with three electrodes, in which the platinum counter-electrode, the reference electrode (calomel), and the working electrode of AZ, AM, YSZ, and bare specimens are immersed in a salt solution containing 50wt% FeCl3 and 50wt% FeSO4. The immersion period of the working electrode before starting the test was considered 30 minutes so as to reach a stable state. Polarization studies were done at a scan rate of 1 mV/s, with the potential range being from -50 mV to +250 mV vs OCP. To collect the device information, PowerSuite Software Version 2/58 was utilized.

2.6 The coating adhesion strength test

The ASTM C633 adhesion strength test is run to assess and determine the bond strength of the coatings, where: 1) the two coated specimens are bonded to the uncoated specimens with high-strength Scotch-Weld 2214 adhesive with a maximum adhesion strength of 70N/mm^2 and 2) the specimens are placed in an oven at 150˚C for two hours. The Zwick Z50 tensile tester is applied. The specimens are subjected to a tensile force at a fixed speed of jaws equal to 1 mm/min. The adhesion strength of the coating is obtained by dividing the maximum force by the cross-sectional area. The accuracy of the results obtained from this test depends on the test conditions, like the specimen alignment with the fixture and the penetration rate of the adhesive into the coating; consequently, the adhesion strength rate is the average adhesion strength obtained from the test on three specimen pairs.

3. Results and discussion

3.1 Coating specifications

-Microstructure and porosity

The cross-sectional microstructure and the thickness of the plasma-sprayed coating are shown in Figure 1, where, as observed, the three coatings do not have layered discretization. The microstructure of the AZ and AM coatings is denser than that of the YSZ. No cracks and layering are observed at the interface of the two coatings. The 9.31% average porosity of YSZ, the 1.7% of AZ, and 1.3% of the AM specimen are bar-charted in Figure 2.

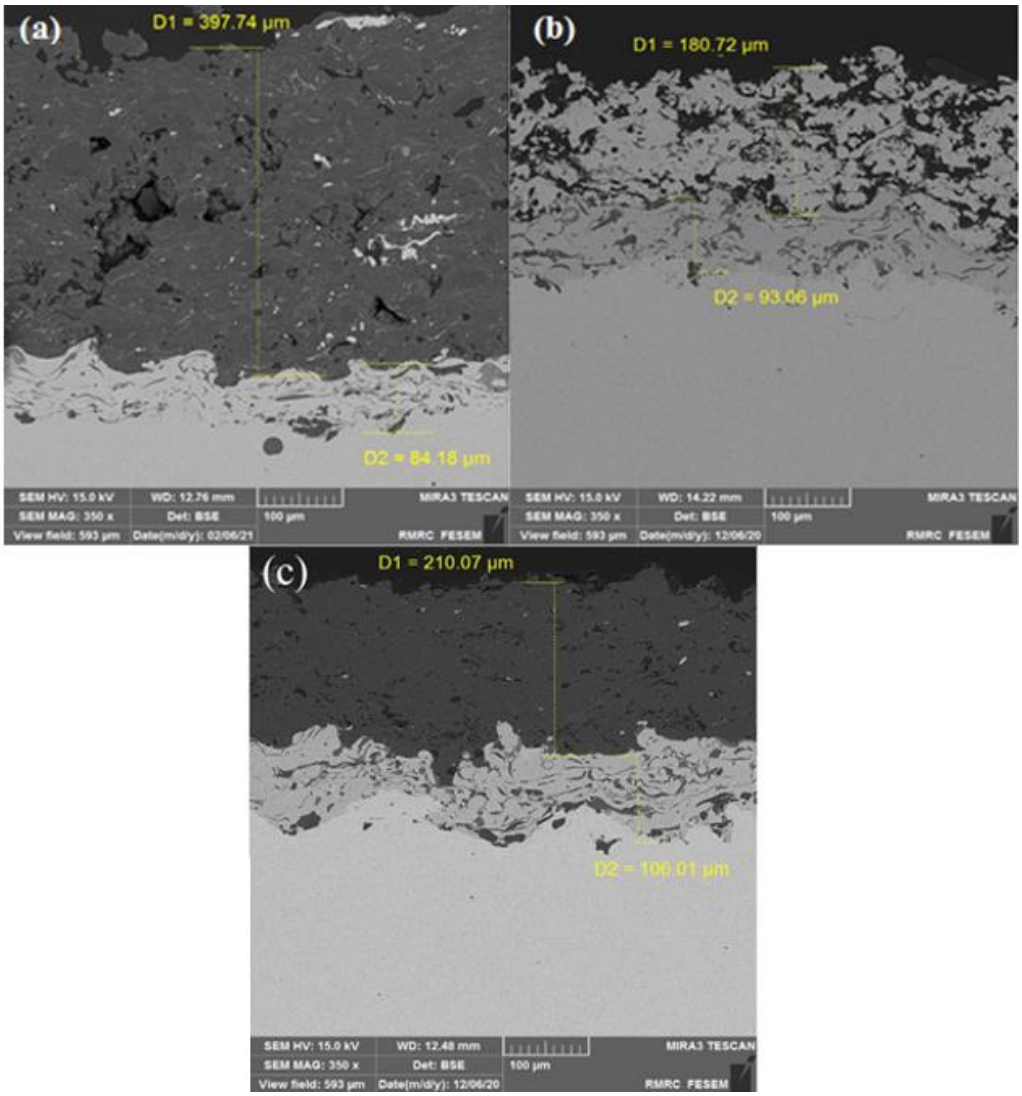

Figure 1. (a) Micrographic structure of the cross-section of AZ coating; (b) Micrographic structure of the cross-section of YSZ coating; (c) Micrographic structure of the cross-section of AM coating

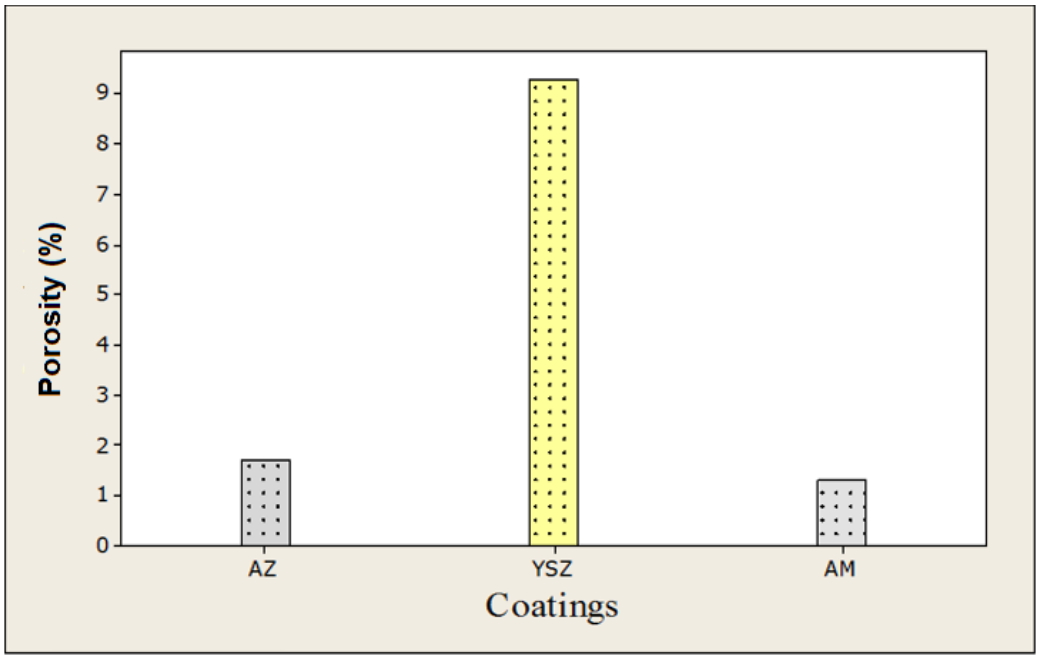

Figure 2. The average porosity of AZ, AM, and YSZ coatings

- Structural analysis of phases

The details of phase analysis of the coating materials are shown in Table 3, where the AZ coating, Corundum phase is a major phase, and the Zirconium Oxide with cubic and mono-clinic structures is a minor phase. As to YSZ coating, the Yttrium-stabilized Zirconium and Zirconium Sulfate are the major and minor phases, respectively. The $MgAl_2O_3$ spinel constitutes the major phase of AM coating.

Table 3. Electrochemical parameters for YSZ, AM, AZ and bare specimens immersed in salt solution of 50wt% $FeCl_3$ and 50wt% $FeSO_4$

Specimen	βa (mV)	-βc (mV)	-Ecorr (mV)	Icorr (μA cm^{-2})
YSZ	417.83	98.28	0.29	0.00029
AM	4680	4660	0.535	0.3384
AZ	17134	23793	1.304	1.107
Bare	1948	1947	0.513	4.474

- The coatings' micro hardness

The porosity of coatings applied by the plasma spray method is relatively high [24]. In general, the micro hardness values are considered an appropriate indicator of homogeneity degree and fusion in the structure. The average hardness values of these coatings are bar-charted in Figure 3, according to which it can be deduced that the lower the porosity, the higher the microhardness of the coating. As per Figures 1 and 2, the average value of microhardness of the AZ and AM coatings is greater than that of YSZ coating, due to their lower porosity.

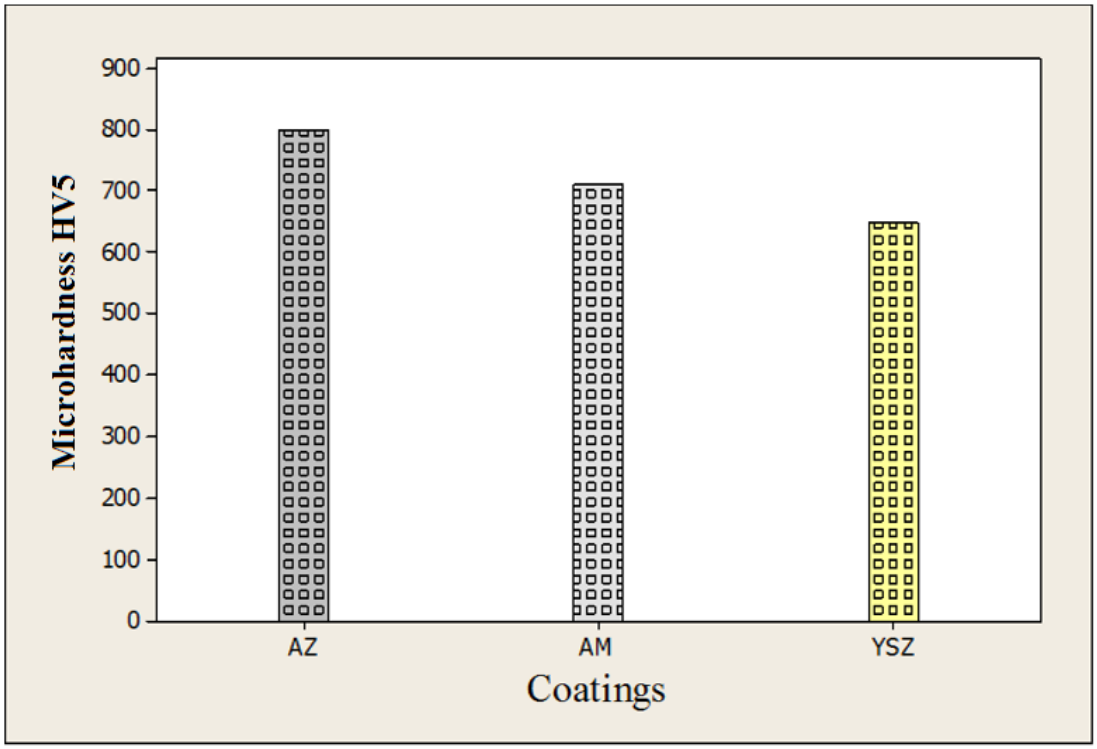

Figure 3. Average micro-hardness of AZ, AM, and YSZ coatings

3.2 Evaluation of the coatings' performance vs. erosion

AM ceramic coating outperforms the AZ, and the AZ ceramic coating outperforms the YSZ. These results are justified by the contribution of zirconia in improving the alumina hardness in the coating's microstructure. According to [26], the hardness of alumina ceramics hardened with zirconia compared to alumina hardness is four-fold. This phenomenon significantly contributes to erosion resistance enhancement. According to[25], YSZ coating has low microhardness due to higher porosity and low toughness[25]. The mass loss of the ceramic coating in (mg) 30 and 90° are bar-charted in Figs. (4 and 5). In all the AZ, AM and YSZ coatings, the maximum average abrasion loss at angles 30° is greater than 90°, which corresponds to the findings in [27].

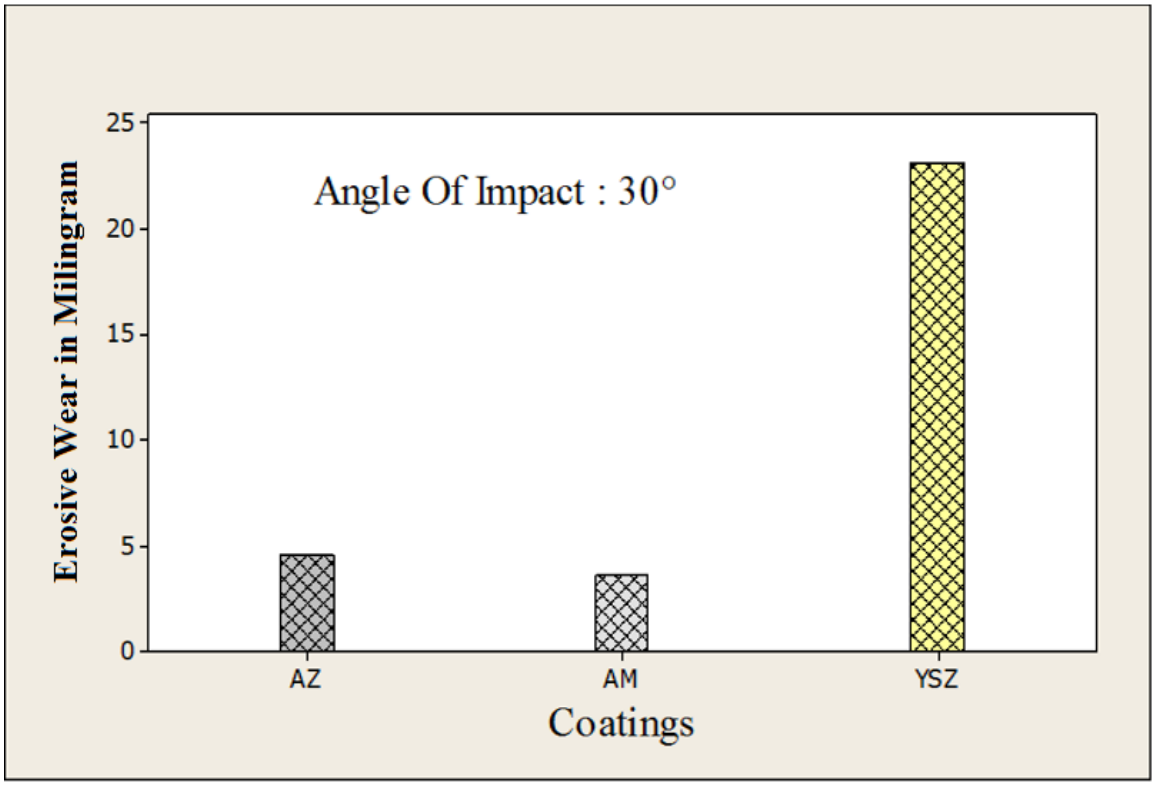

Figure 4. Coatings' average erosion based on the mass loss in mgr at a 70 m/s impact speed on the coating surface at 30˚

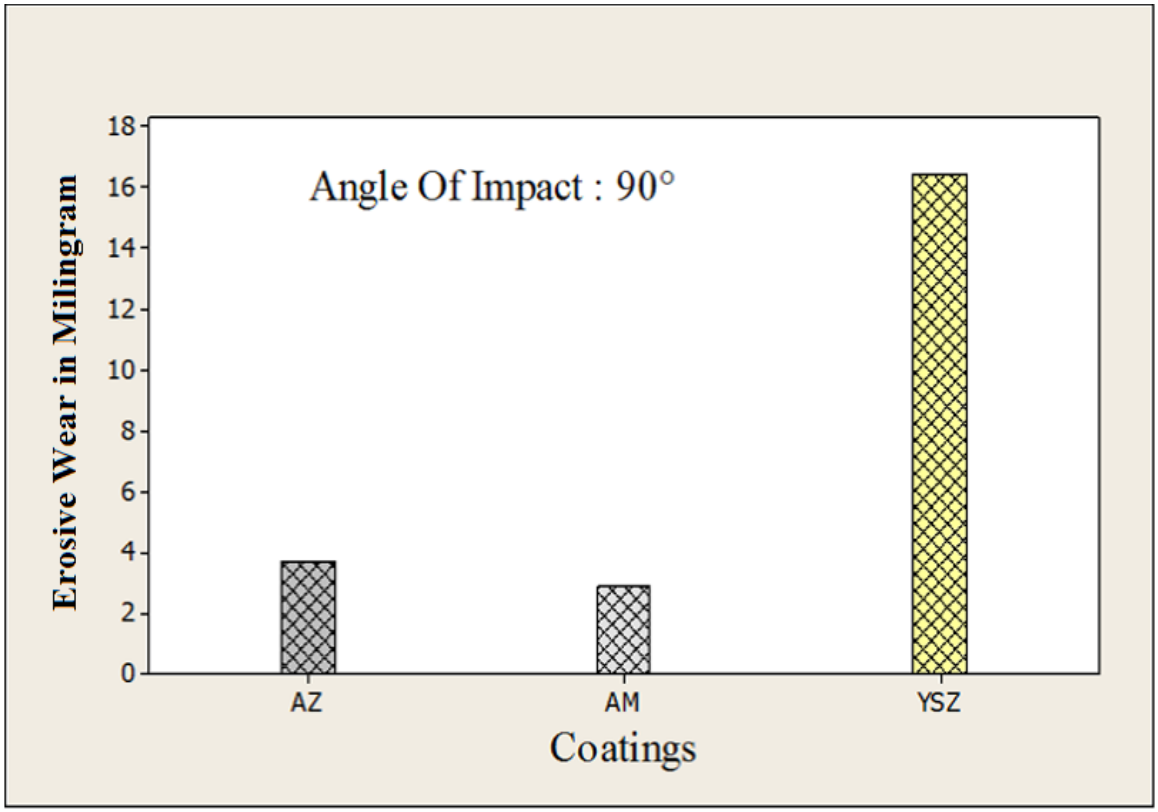

Figure 5. Coatings' average erosion based on the mass loss in mg at a 70 m/s impact on the coating surface at 90˚

3.3 Evaluation of hot chemical corrosion

The X-ray diffraction peaks before and after placing the AZ, AM, and YSZ specimens into the furnace are shown in Figs. (6, 7, 8, 9 10 and 11), where, as observed, a Fe_2O_3 peak appears in both coatings after specimens are put into the furnace. According to Equation 1 [10], the Fe_2O_3 phase is formed through the reaction between $FeCl_3$ and $FeSO_4$, indicating that no reaction occurs between $FeSO_4$ and $FeCl_3$ and the coatings. The brown-colored areas in Figure 12 exhibit the Fe_2O_3 formation on the coating's surface after being put into the furnace.

$$FeCl_3(s) + FeSO_4(s) + 1/2O_2(g) \rightarrow Fe_2O_3(s) + 3/2Cl_2(g) + SO \quad (1)$$

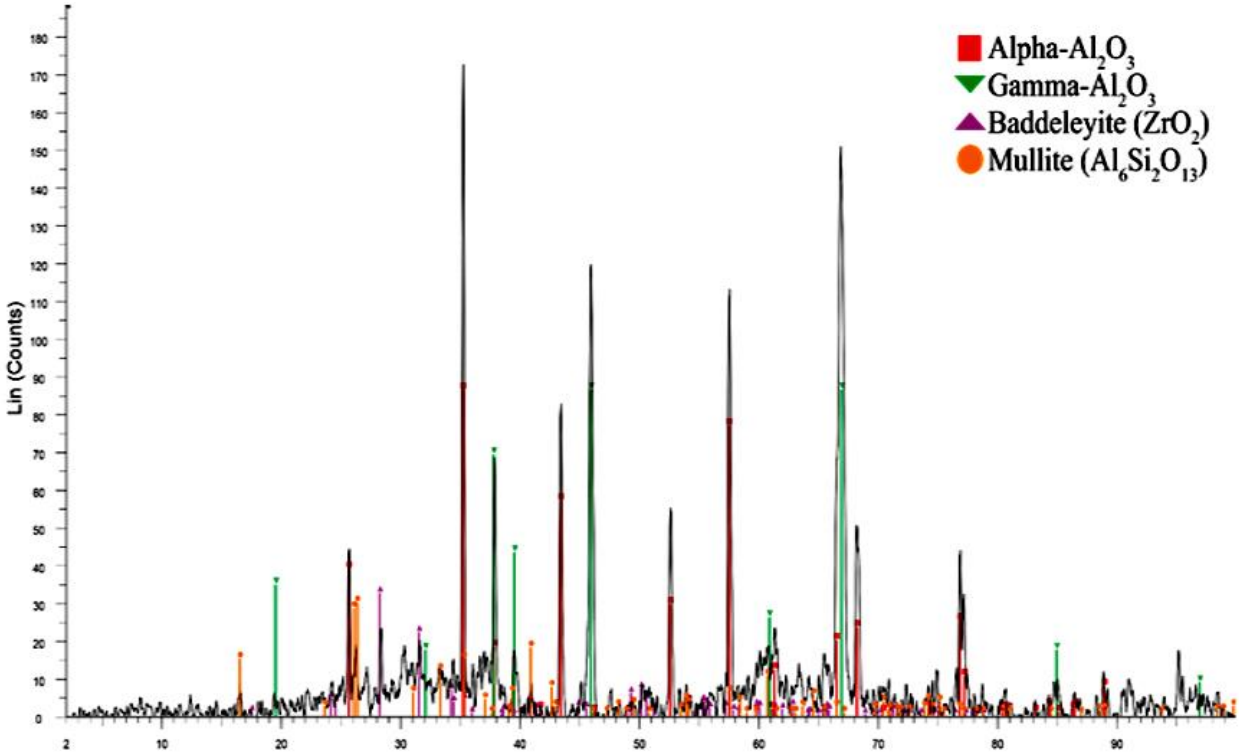

Figure 6. X-ray diffraction before placing the AZ specimens into the furnace

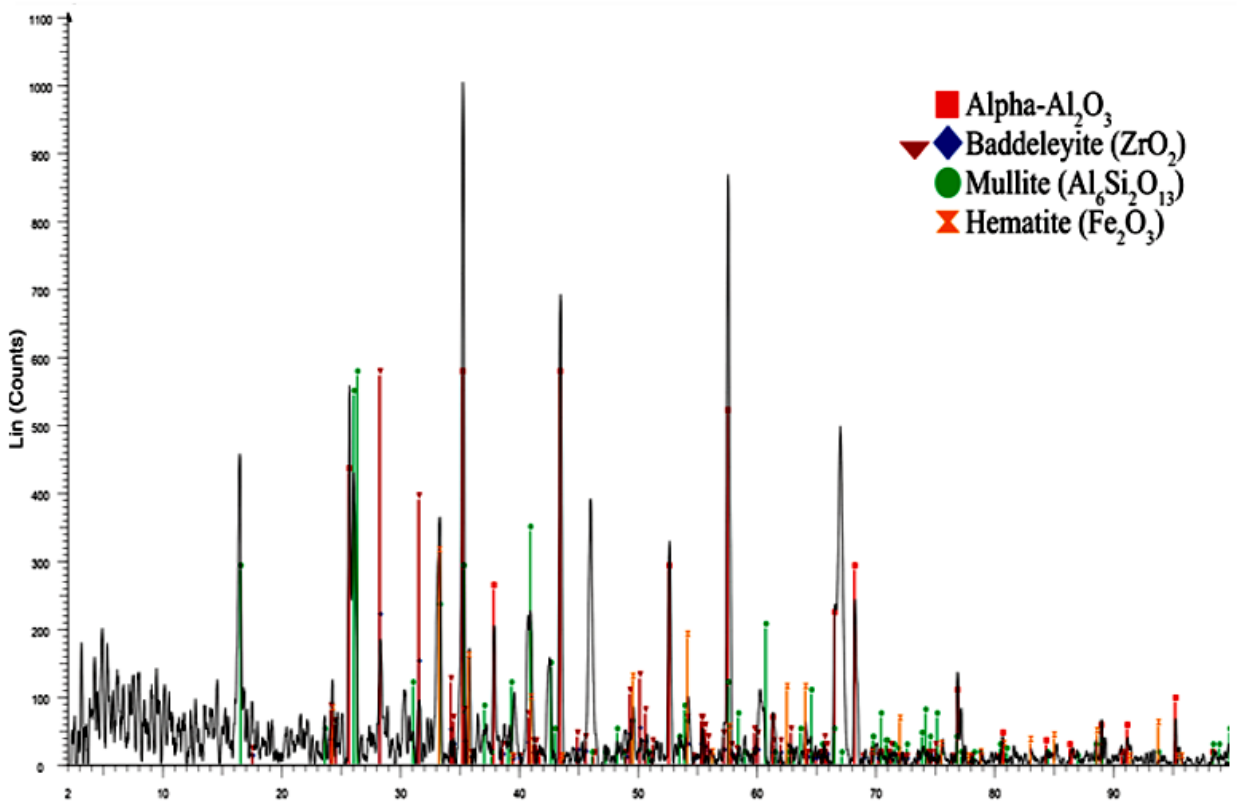

Figure 7. X-ray diffraction after placing the AZ specimens into the furnace

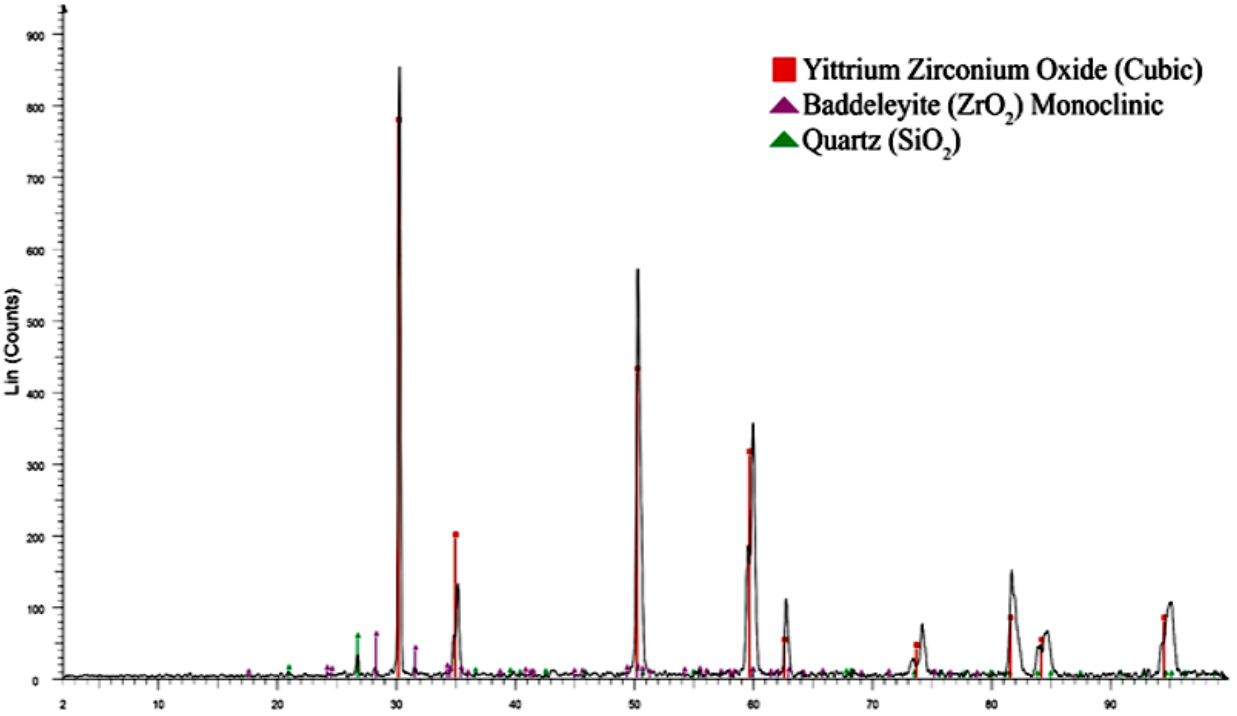

Figure 8. X-ray diffraction before placing the YSZ specimens into the furnace

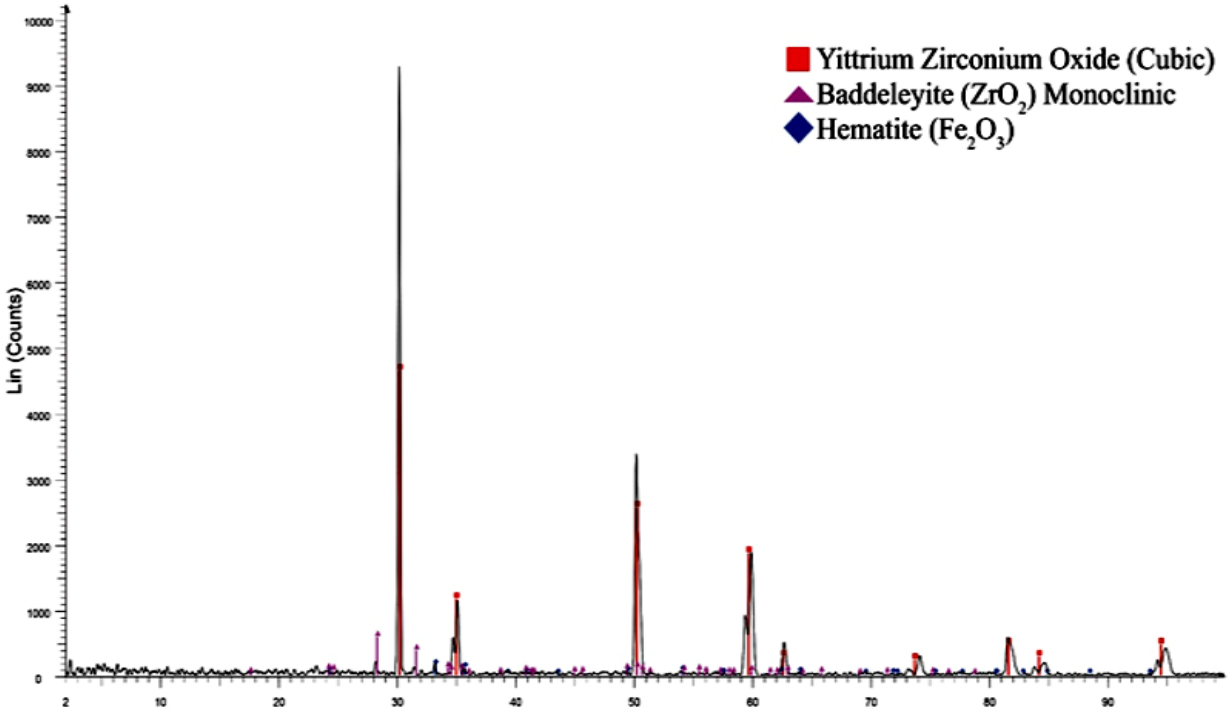

Figure 9. X-ray diffraction after placing the YSZ specimens into the furnace

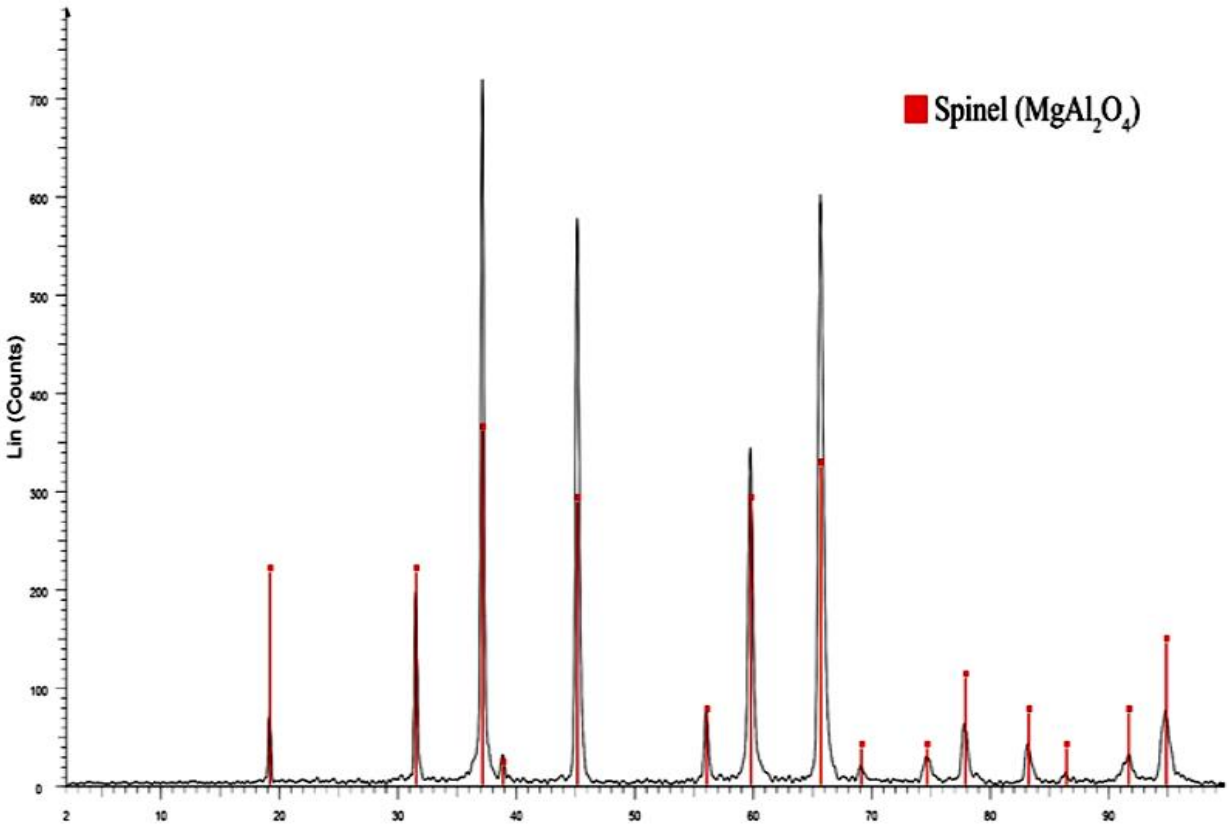

Figure 10. X-ray diffraction before placing the AM specimens into the furnace

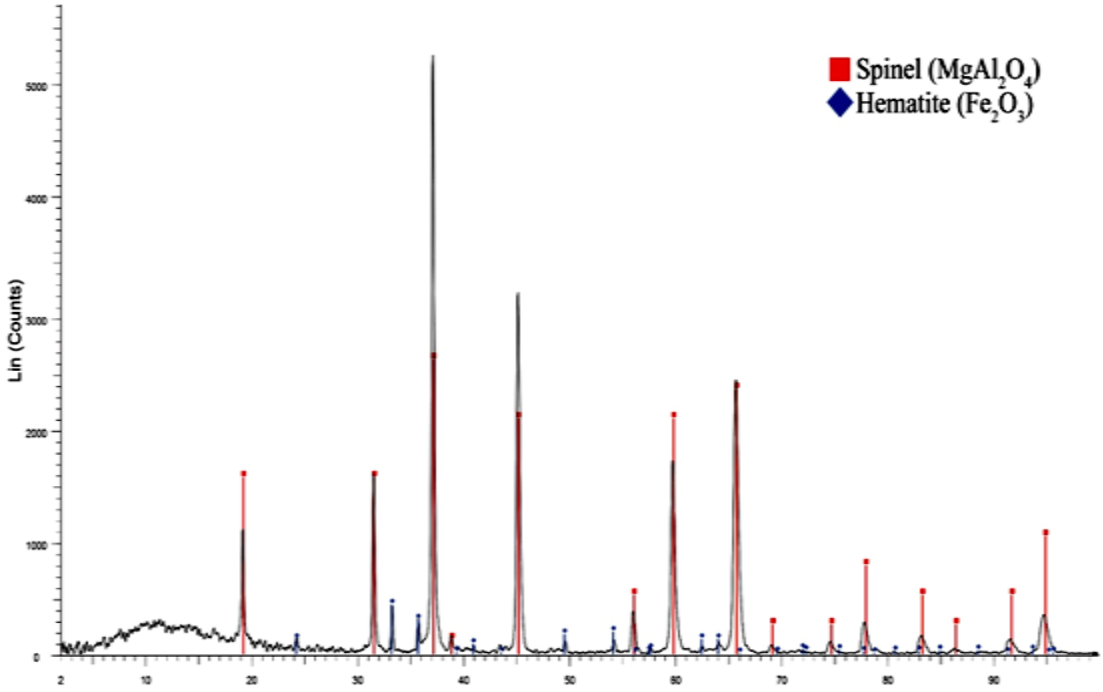

Figure 11. X-ray diffraction after placing the AM specimens into the furnace

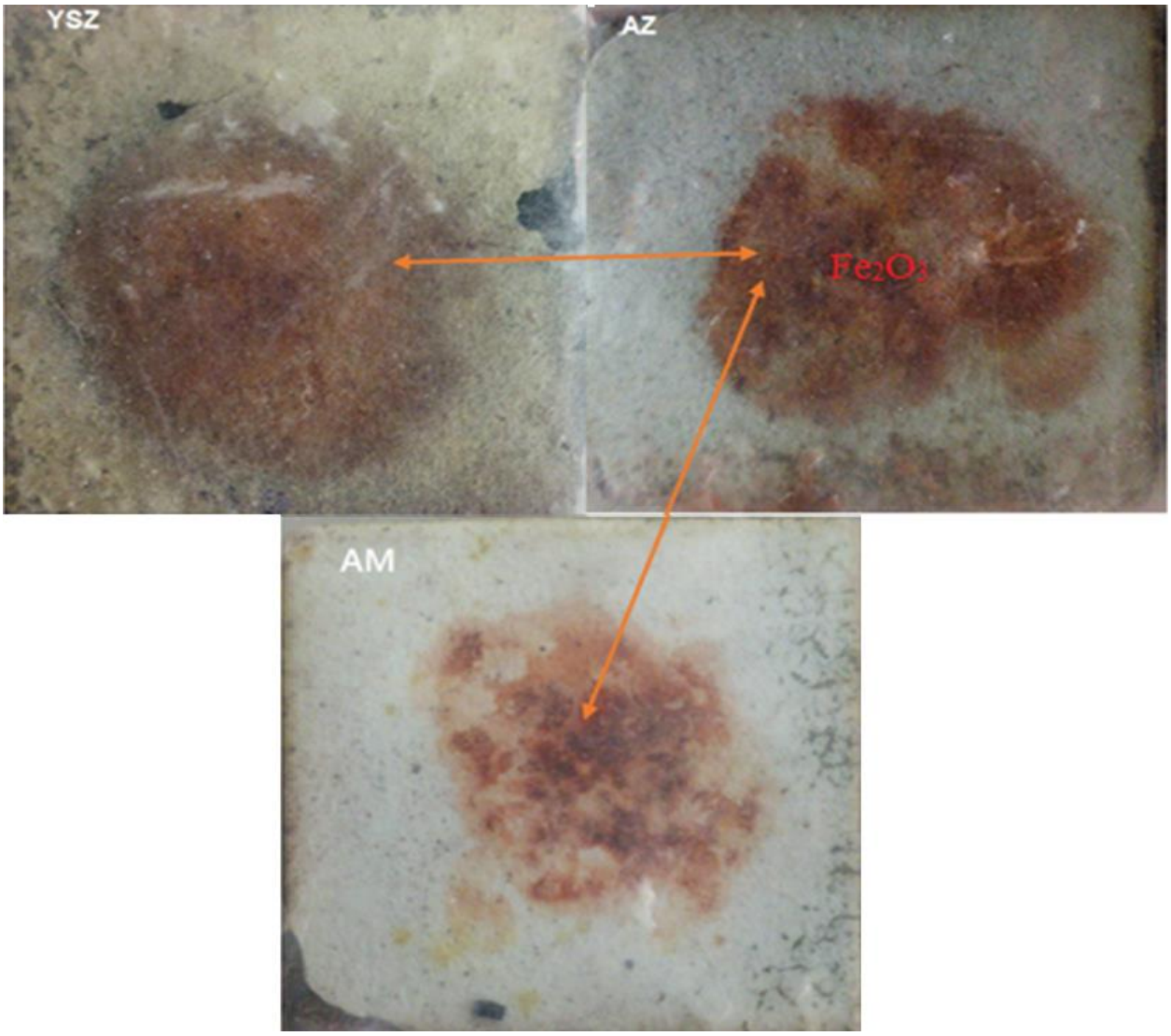

Figure 12. Specimens of AZ, AM, and YSZ coatings after chemical hot corrosion test

3.4 Electrochemical tests

- Polarization test

According to Table 4, the YSZ specimen immersed in a salt solution of 50wt% FeCl3 and 50wt% FeSO4 has a very low corrosion current of 0.00029 microamperes/cm2. Hence, compared to the bare specimen with a current density of 4.474 microamperes/cm2, the YSZ specimen has better protection against corrosion and oxidation under the same conditions. Further, AM and AZ specimens outperform the bare specimen in terms of protection against corrosion in the same immersion conditions. These results confirm the good interaction of the coated layer of YSZ, AM, and AZ specimens with the copper substrate. Corrosion current densities are estimated based on the extrapolation of anode and cathode Tafel lines, the diagram of which has been displayed in Figure 13.

Table 4. XRD analysis of the coating materials phases

Coating	Coating Phases
AZ	Corundum Al_2O_3 Aluminum Oxide (Al_2O_3), Zirconium Oxide ZrO_2 Cubic, Zirconium Oxide ZrO_2 Monoclinic
YSZ	Zirconium Yttrium Oxide Zr0.9Y0.1O1.95, Zircon $Zr(SiO_4)$
AM	$MgAl_2O_4$

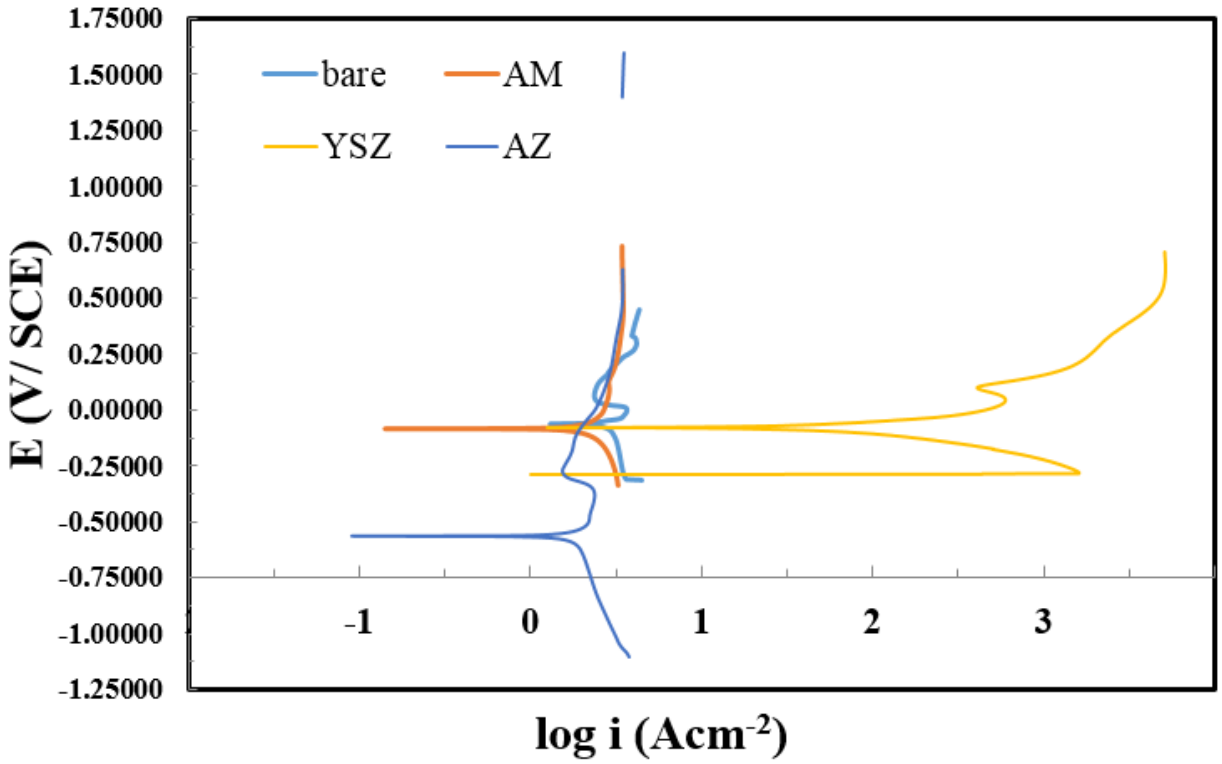

Figure 13. The polarization test of YSZ, AM, AZ, and bare specimens immersed in a salt solution of 50%wt% $FeCl_3$ and 50wt% $FeSO_4$.

3.5 The mechanical wear test

This test is run to assure the coating scratch resistance when installing the blast tuyere. In this test, AZ coating undergoes higher abrasion resistance compared to YSZ. The results of this test are bar-charted in Figure 14 and termed the mass loss average.

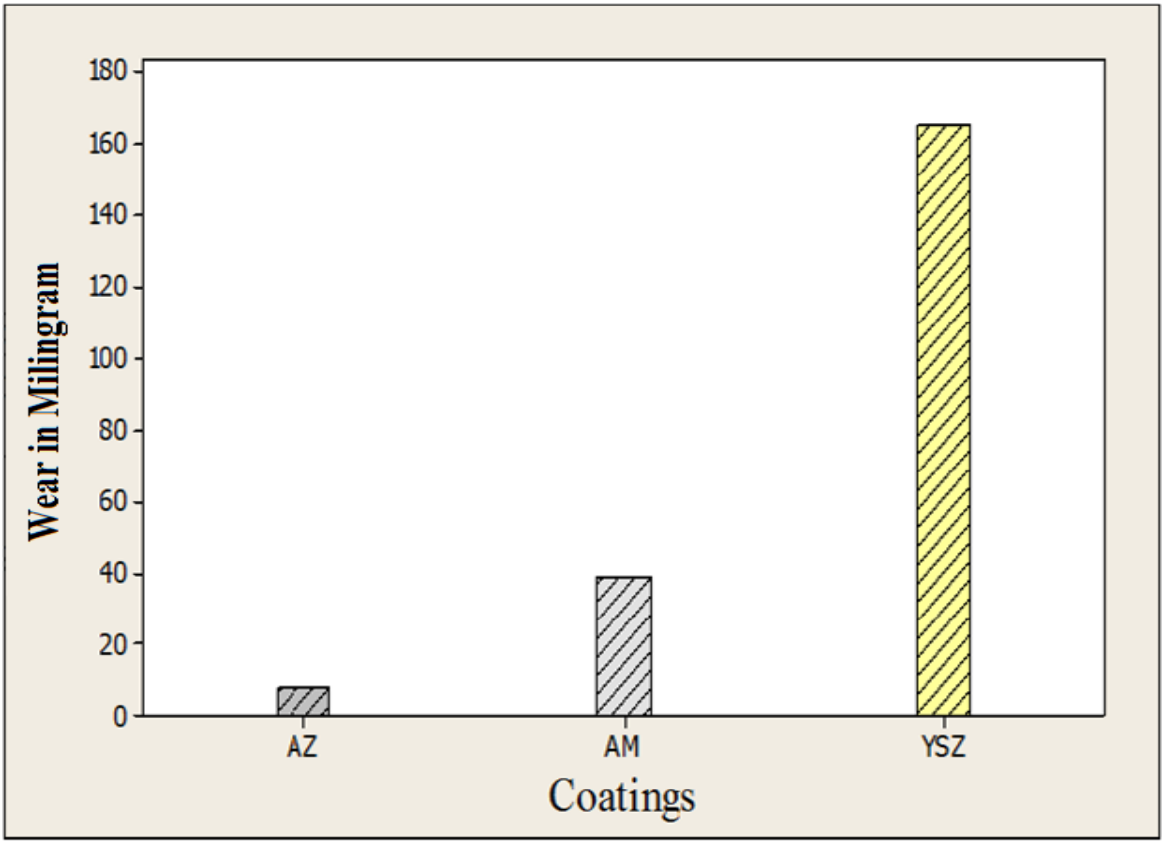

Figure 14. Mass loss average based on the mechanical abrasion test of AZ, AM, and YSZ coatings

3.6 Evaluation of adhesion strength test results

The results of the adhesion strength test are bar-charted in Figure 15, where, as observed, the AZ coating adhesion strength is lower than the YSZ coating (up to 20%). Still, the adhesion strength of AZ coating can be deemed close to that of YSZ coating.

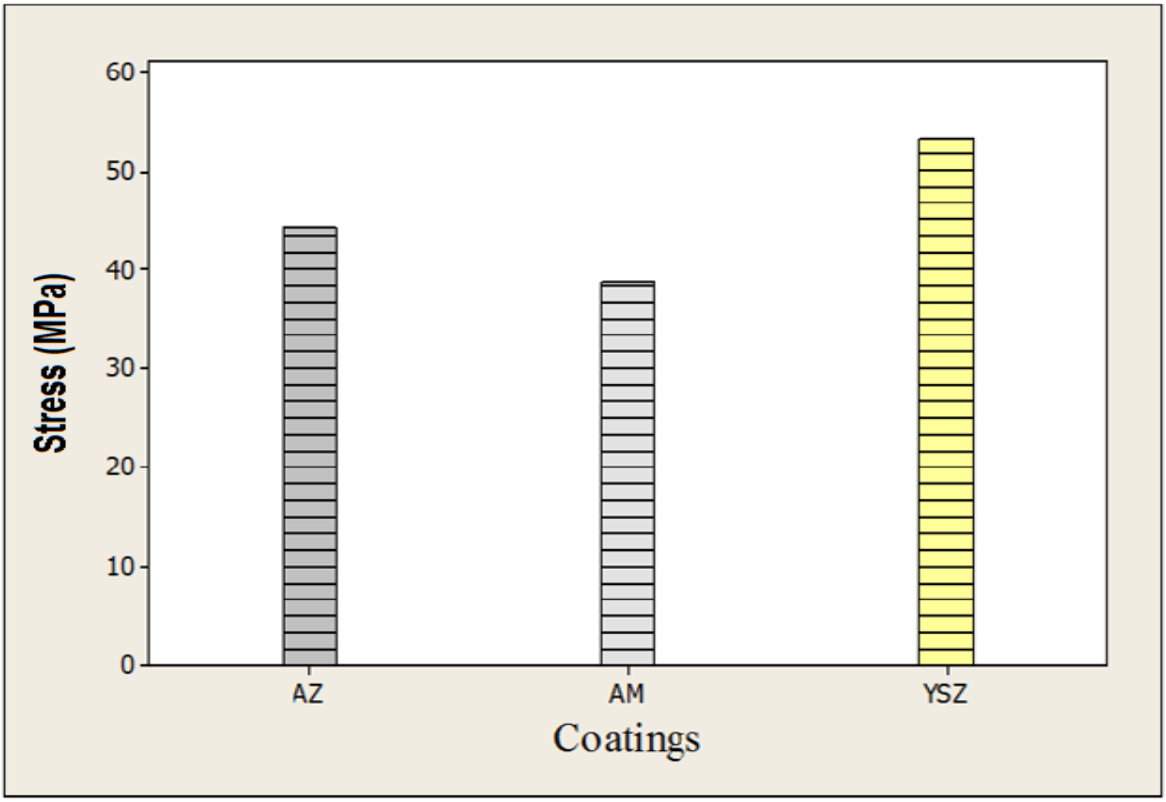

Figure 15. AZ, AM, and YSZ coatings' adhesion strength average in MPa

3.7 Assessing the coatings

After running these tests on AM and AZ coatings and a relatively complete assessment of the conditions and coatings' performance, the specifications of the AM and AZ coatings are assessed. For comparison, the same tests are run on the YSZ coating as the reference, with the results presented in Table 5.

Table 5. Performance comparison of coatings in different tests

Specifications / Test	AZ Coating	AM Coating	YSZ Coating	Suitable Coating with better performance	Percentage of the coating with better performance compared to other two coatings		
					AM	AZ	YSZ
Micro Hardness (V)	801	711.2	649	AZ	12.6		23
Porosity (%)	1.7	1.3	9.31	AM		31	716
Mechanical Erosion at Impact Angle 90˚ (mgr)	3.7	0.8	16.5	AM		462	2062
Mechanical Erosion at Impact Angle 30˚ (mgr)	4.6	3.63	22.7	AM		26	625
Chemical Hot Corrosion	None	None	None	YSZ, AZ, AM	Similar	Similar	Similar
Mechanical Wear (mgr)	8	29.9	164.6	AZ	73		2058
Adhesion Strength (MPa)	44.4	38.6	53.43	YSZ	38	23	23

3.8 Experimental evaluation of the coatings on air tuyere of blast furnace

There exist many studies on different ceramic coatings applied on the blast air tuyere, but what lacks is a study on the adhesion strength of the coating, an essential component in metallurgy. The adhesion strength prevents the premature detachment and degradation of the coating layers and enhances the coating service life, thus, extending the service life.

Under severe operating conditions in the furnace, the BF tuyere experiences chemical and mechanical corrosion. Another factor contributing to the tuyere failure is burnout due to the wettability of tuyere due to hot metal penetration into the copper nose of the tuyere outer body (Figure 16). Chemical corrosion is mainly caused by the acidic gases emitted from Sulphur and chlorine, as the products of coke and/or coal reactions in BF. Mechanical corrosion occurs as a result of material particle motion, especially coke particles, due to the eddy current. (Figure 17). To calculate the mechanical erosion rate, Equation 1, is applied. Accordingly, the corrosion rate is calcaulted directly proportional to the weight loss volume and inversely proportional to the eroded material density, cross-sectional area, and exposure time (Equation 2) [23].

$$Corrosion\ Rate\ (\mathrm{mm/year}) = 87.6 \times 10^3 \left(\frac{w}{DAT}\right) \quad (2)$$

where,

W = weight loss in mg

D = Density in g/cm^3

A= Sample area in cm^2

T = Immersion time in hr

87.6 = Corrosion's calculation constant in mm/year

A summary of parameters and their symbols is described in Table 6 for further reference.

Table 6. Symbols and abbreviation

Symbol	Description
BF	Blast Furnace
YSZ8%	Yttria Stabilized Zirconia
AZ	Alumina-Zirconia
AM	Alumina-Magnesia
β_a(mV)	Anodic Tafel Slope
- βc(mV)	Cathodic Tafel Slope
- E_{cor}r(mV)	Corrosion Electric Potential
I_{corr} (μA cm^{-2})	Corrosion Intensity Current
W	weight loss in mg
D	Density in g/cm^3
A	Sample area in cm^2
T	Immersion time in hour

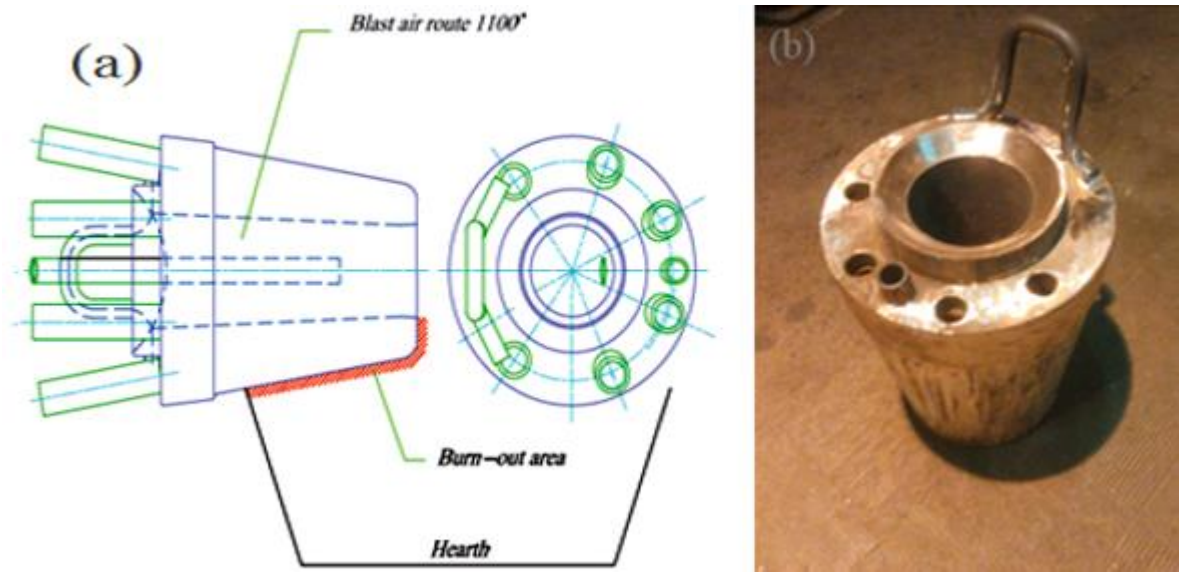

Figure 16. (a) Blast air tuyere and the area exposed to burning damage (b) Blast air tuyere

Figure 17. The areas damaged by mechanical and chemical hot corrosion and burning on the body and nose of the tuyere

According to Table 5 and the qualitative and quantitative comparison of the tests, it can be deduced that AZ and AM are the proper materials to be consumed as BF tuyere coating. Therefore, a three-layer coating consisting of a NiCrAlY bond layer with a thickness of 100-120 microns and two ceramic AZ layers, each 150 microns thick, is applied on one BF blast air tuyere. Likewise, the AM coating is applied on a damaged tuyere. After 45 days, it is replaced, while the tuyere with AZ coating is replaced after 170 days because of the blast air passage blockage by slag and molten cast iron produced during blast furnace abnormal operating conditions. No damage was detected on the body and outer nose of the tuyere coated with AZ. The AM and AZ coatings after being damaged and taken out from the blast furnace are shown in Figures 18 and 19, respectively. The top coatings are highly contributive in protecting the underlying layers and substrates. Any damage in the topcoat would initiate the bonding layer and the substrate damage. Based on field studies, the lower part of the tuyere's tip is mainly damaged by high heat due to hot metal wettability. The mechanical corrosion, erosion, and hot chemical corrosion are the primary factors contributing to the tuyere's upper parts damage.

Figure 18. Newly developed tuyere with AM coating after damage and removal from the blast furnace

Figure 19. Newly developed tuyere with AZ coating after the blast air passage filled up with the melt and removal from the blast furnace

4. Conclusions

The ceramic powder coatings, AZ, AM, and YSZ, are plasma sprayed on a 99.99% copper substrate to compare their performance. The adhesion strength of the AZ coating is almost similar to that of the YSZ coating, with its average adhesion strength of 20% lower than the YSZ coating. The adhesion strength of the AM coating is lower than the YSZ coating at 38%. The findings of this study are briefed as follows:

- The AZ and AM coatings perform similarly to the YSZ coating in the hot chemical corrosion test. After the test, no new chemical composition is formed on the surface of the three coatings by the coating reaction
- The mechanical corrosion rate obtained for AZ, AM, and YSZ specimens through Equation 2 is 739.89, 579.03, and 3731.56 gr/year, respectively
- In the mechanical erosion test, the AM coating outperforms the YSZ and AZ coatings at 90˚, while at an angle of 30˚, its performance is relatively better than AZ coating and appropriate compared to YSZ coating
- In the mechanical Wear test, the AZ coating outperforms AM and YSZ coatings
- To evaluate the AZ and AM coatings' performance subject to actual operating conditions of the blast furnace through the field test, a three-layer ceramic coating, consisting of a NiCrAlY bond layer 100 to 120 microns thick and two AZ ceramic layers, each 150 microns

thick, is applied on one BF's tuyere. The AM ceramic coating is similarly applied on another tuyere. The prepared specimens were simultaneously installed at Esfahan Steel Co.'s (ESCO) blast furnace No.2. The tested coating was finally installed in BF

- The tuyere with AM coating is damaged after 45 days and replaced, while the tuyere with AZ coating is replaced after 170 days only due to the blast air passage blockage by slag and molten cast iron produced during blast furnace abnormal operating conditions. No damage was detected on the body and outer nose of the tuyere
- Based on the findings, the AZ coating is expected to be an appropriate coating for the blast furnace tuyere considering the metallurgical, mechanical, and thermal properties

5. References

[1] Chatterjee, R., Nag, S., Kundu, S., Ghosh, U. and Singh, U. 2021. A journey towards improving tuyere life. Transactions of the Indian Institute of Metals. 74(5): 1-12. doi:10.1007/s12666-021-02203-y.

[2] Gao, T., Jiao, K., Zhang, J. and Ma, H. 2020. Melting erosion failure mechanism of tuyere in blast furnace. ISIJ International. 61(1): 71-78. doi:10.2355/isijinternational.ISIJINT-2020-138.

[3] Agrawal, A., Tiwari, R.K., Kumar, S., Chatterjee, R., Singh, B.K., et al. 2020. Technological advancements in evaluating the performance of the pulverized coal injection through tuyeres in blast furnace. Metallurgical Research & Technology. 117(6): 611-611. doi:10.1051/metal/2020068.

[4] Farkas, O. and Móger, R.J.s.r.i. 2013. Metallographic aspects of blast furnace tuyere erosion processes. Steel Research International. 84(11): 1171-1178. doi:10.1002/srin.201200328.

[5] Matsumura, Y. and Taoka, K. 2013. Tuyere structure of melting furnace. US Patetnt. US20100320653A1.

[6] Chatterjee, R., Nag, S., Kundu, S., Chakraborty,R., Singh,U. and Chandra, S. 2019. Erosion Behavior of Blast Furnace Tuyere. ISIJ International. 59(9):1732-1734. doi:10.2355/isijinternational.ISIJINT-2018-710.

[7] Mori, K., Yamada, T., Nakamoto, K., Kato, T., Onaka, H. and Yamamoto, T. 1974. Heat insulating durable tuyere. Official Gazette of the United States Patent Office.

[8] Portnov, L.V., Nikitin, L.D., Bugaev, S.F. and Shchipitsyn. 2014. Improving the durability of blast-furnace tuyeres. Metallurgist. 58(5-6): 488-491. doi:10.1007/s11015-014-9938-7.

[9] Kirillova, N.L., Radyuk, A.G., Titlyanov, A.E. and Gorbatyuk. 2013. Improving air-tuyere operation in blast furnaces by means of coatings and sealant. Steel in Translation. 43(5): 231-235. doi:10.3103/S0967091213050082.

[10] Pathak, A., Sivakumar, G., Prusty, D., Shalini, J., Dutta, M. and Joshi, S. V. 2015. Thermal spray coatings for blast furnace tuyere application. Journal of Thermal Spray Technology. 24(8):1429-1440. doi:10.1007/s11666-015-0350-z.

[11] Tarasov, Y.S., Kobelev, O.A. and Sayfullayev, S.D. 2020. Improving the heat insulation efficiency of the blast furnace tuyere. Proc. IOP Conference Series: Materials Science and Engineering. 971:032034. doi:10.1088/1757-899X/971/3/032034.

[12] Zhang, D., Gong, S., Xu, H. and Guo, H.J.V. 2003. Measurements of the thermal gradient over EB-PVD thermal barrier coatings. Vacuum. 70(1): 11-16. doi:10.1016/S0042-207X(02)00509-2.

[13] Zhang, Z., Chen, H., Wang, Y., Wang, G., Li, L., Zhong, M. and Bai, H. 2022. Effect of sodium silicate binder on the performance of ceramic coatings on copper prepared by the slurry method. Surface and Coatings Technology. 448: 128868. doi:10.1016/j.surfcoat.2022.128868.

[14] Li, C.-J., Luo, X.-T., Yao, S.-W., Li, G.-R., Li, C.-X. and Yang, G.-J. 2022. The bonding formation during thermal spraying of ceramic coatings: A review. Journal of Thermal Spray Technology. 31(4): 780-817. doi:10.1007/s11666-022-01379-z.

[15] Varghese, P., Vetrivendan, E., Krishnan, R., Mathews, T. and Ningshen, S. 2021. Plasma sprayed alumina-yttria composite ceramic coating for electrical insulation applications. Surface and Coatings Technology. 405: 126566. doi:10.1016/j.surfcoat.2020.126566.

[16] Junge, P., Greinacher, M., Kober, D., Stargardt, P. and Rupprecht, C. 2022. Metastable phase formation, microstructure, and dielectric properties in plasma-sprayed alumina ceramic coatings. Coatings. 12(12): 1847. doi:10.3390/coatings12121847.

[17] Manoj, A., Basha, M., Basha, S. and Sankar, M. 2021. A review-black oxide coating on metal substrates of steels, aluminium, magnesium and copper. Advances in Science and Technology. 106: 46-53. doi:10.4028/www.scientific.net/AST.106.46.

[18] Liu, G., Zhong, X., Xing, Y., Li, T. and Pan, W. 2021. Surface resistivity and bonding strength of atmosphere plasma sprayed copper-coated alumina substrate. Journal of the American Ceramic Society. 104(3): 1193-1197. doi:10.1111/jace.17522.

[19] Skripalenko, M.M., Kobelev, O.A. and Sayfullayev, S.D. 2020. Burnout resistance assessment of air tuyere in blast furnace. IOP Conference Series: Materials Science and Engineering. 971(3): 32033. doi:10.1088/1757-899X/971/3/032033.

[20] Nakahira, H. 1976. Blast-furnace tuyere having excellent thermal shock resistance and high durability. US Patetnt. US3977660A.

[21] Chesters, J.H. 1973. Refractories--production and properties. Iron and Steel Institute. CRC Press. London.

[22] Stevens, R. 1983. An introduction to zirconia. Magnesium Elektron Limited.

[23] Fontana, M.G. and Greene, N.D. 1967. Corrosion engineering. McGraw-Hill Book Company.

[24] Xu, H., Guo, H. and Gong, S. 2008. Thermal barrier coatings. Woodhead Publishing Series in Metals and Surface Engineering.

[25] Davis, J.R. 2004. Handbook of thermal spray technology. ed. ASM international,

[26] Claussen, N. 1976. Fracture toughness of Al2o3 with an unstabilized ZrO2 dispersed phase. Journal of the American Ceramic Society. 59(1-2): 49-51. doi:10.1111/j.1151-2916.1976.tb09386.x.

[27] Ćurković, L., Kumić, I. and Grilec, K. 2011. Solid particle erosion behaviour of high purity alumina ceramics. Ceramics International. 37(1): 29-35. doi:10.1016/j.ceramint.2010.08.029.